

**PIP<sub>2</sub> stabilises active states of GPCRs and enhances the selectivity  
of G-protein coupling**

**Hsin-Yung Yen<sup>1,2</sup>, Kin Kuan Hoi<sup>1</sup>, Idir Liko<sup>1,2</sup>,  
George Hedger<sup>3</sup>, Michael R. Horrell<sup>3</sup>, Wanling Song<sup>3</sup>, Di Wu<sup>1</sup>, Philipp Heine<sup>4</sup>,  
Tony Warne<sup>5</sup>, Yang Lee<sup>5</sup>, Byron Carpenter<sup>5,†</sup>, Andreas Plückthun<sup>4</sup>,  
Christopher G. Tate<sup>5</sup>, Mark S. P. Sansom<sup>3\*</sup>, Carol V. Robinson<sup>1\*</sup>**

**Affiliations:**

<sup>1</sup>Chemical Research Laboratory, South Parks Road, University of Oxford, OX1 3QY, U.K.

<sup>2</sup>OMass Technologies Ltd., Begbroke Science Park, Woodstock Rd, Yarnton, Kidlington OX5 1PF, U.K.

<sup>3</sup>Department of Biochemistry, South Parks Road, University of Oxford, OX1 3QU, U.K.

<sup>4</sup>Biochemisches Institut, Universität Zürich, Winterthurerstr. 190 CH-8057, Zürich, Switzerland.

<sup>5</sup> MRC Laboratory of Molecular Biology, Francis Crick Avenue, Cambridge Biomedical Campus, Cambridge CB2 0QH, U.K.

\*Correspondence to: mark.sansom@ bioch.ox.ac.uk and carol.robinson@chem.ox.ac.uk.

† Current address: Warwick Integrative Synthetic Biology Centre, School of Life Sciences, Gibbet Hill Campus, The University of Warwick, Coventry, UK

**G protein-coupled receptors (GPCRs) are involved in many physiological processes and are therefore key drug targets <sup>1</sup>. Despite detailed structural information however the effects of lipids on the receptors themselves, or on their downstream coupling to G proteins, are ill defined. Here we use native mass spectrometry to identify endogenous lipids bound to three class A GPCRs. We demonstrate preferential binding of phosphatidylinositol 4,5 bisphosphate (PIP<sub>2</sub>) over related lipids and confirm hotspots for PIP<sub>2</sub> binding on the intracellular face of the receptors. Endogenous lipids were also observed bound directly to the entire adenosine A<sub>2A</sub> receptor (A<sub>2A</sub>R) trimeric G<sub>αs</sub>βγ protein complex in the gas phase. Recruiting engineered G<sub>α</sub> subunits (mini-G<sub>s</sub>, i, 12) <sup>2</sup> we found that the β<sub>1</sub>AR: mini-G<sub>αs</sub> complex is stabilised by the binding of two PIP<sub>2</sub> molecules. By**

**contrast PIP<sub>2</sub> did not stabilise coupling between  $\beta_1$ AR and other G $\alpha$  subunits (mini- G $\alpha_{i,12}$ ) or a high affinity nanobody. Other endogenous lipids that bound to receptors showed no effect on coupling, highlighting the specificity of PIP<sub>2</sub>. Potential of mean force calculations and increased GTP turnover of the activated neurotensin receptor: trimeric G $\alpha_i\beta\gamma$  complex in the presence of PIP<sub>2</sub> further support the specific effect of PIP<sub>2</sub> on coupling. Together our results identify key residues on cognate G $\alpha$  subunits that mediate simultaneous PIP<sub>2</sub> bridging interactions between basic residues on class A receptors, which do not correspond with those on class B GPCRs. By uncovering the effects of lipid modulation of receptors we highlight consequences for understanding function, G protein selectivity and drug targeting of class A GPCRs.**

The emerging view from biophysical studies of GPCRs is that they exist as ensembles of discrete conformations that can be influenced by ligands, regulatory proteins, pH and ions as well as potentially lipid molecules<sup>3</sup>. The role of these conformational ensembles in signaling pathways are further compounded by the combinatorial effects of the multiple distinct heterotrimeric complexes formed from 21 G $\alpha$ , 6 G $\beta$  and 12 G $\gamma$  subunits. Investigating the relationship between GPCRs, small molecule modulators and numerous binding partners is challenging therefore, due to the difficulties of observing the complexity of these interactions directly. A previous study characterized lipid interactions with  $\beta_2$ AR in high-density lipoparticles<sup>4</sup> to which phospholipids were added exogenously. However, the selectivity and the effects of different phosphatidylinositol phosphate (PIP) lipids on downstream coupling were not explored. Here we develop and apply high-resolution native MS to interrogate endogenous lipid - receptor interactions<sup>5,6</sup> for three class A GPCRs (the  $\beta_1$ -adrenergic receptor ( $\beta_1$ AR), the adenosine A<sub>2A</sub> receptor (A<sub>2A</sub>AR) and the neurotensin receptor 1 (NTSR1)). We discover novel effects of PIP<sub>2</sub> that stabilise these receptors in active states, increase GTPase activity and enhance selectivity of coupling to G-proteins.

We considered first the endogenous lipids that bind directly to  $\beta_1$ AR and the stabilised NTSR1 HTGH4- $\Delta$ IC3B<sup>7</sup> expressed and purified from insect cells and *E. coli* respectively. Peaks corresponding to lipid adducts were observed for  $\beta_1$ AR and for NTSR1 (Fig. 1a and Extended Data Fig. 1a). Collisional dissociation of protein-lipid complexes allowed us to identify two major classes of lipids the phosphatidylserines (PS) (34:2 and 36:2) and phosphatidylinositol phosphates (PI(4)P) (42:5) bound to  $\beta_1$ AR as well as phosphatidic acid (PA) (36:2) bound to NTSR1. The (Extended Data Fig. 1b and 1c and Extended Data Table 1). Investigating further this selectivity we incubated NTSR1 with PA as well as other anionic lipids (PS and PI), a zwitterionic lipid (PC), and a neutral lipid (DAG). Mass spectra showed that NTSR1 interacts preferentially with PA, PS and PI (Extended Data Fig. 2a-2e). We did not observe significant binding of PG although a positive impact on G protein activation of NTSR1 has been reported for PG in a nanodisc<sup>8</sup>. It is possible that PG could affect the local net charge at the receptor/lipid interface. Similarly  $\beta_1$ AR, when incubated with detergent-solubilised PS (16:0-18:1) or phosphatidylinositol 4-phosphate (PI(4)P) (18:1-18:1), showed higher affinity toward PI(4)P than PS (Fig. 1a and Extended Data Fig. 2f and 2g).

To probe the selectivity of different PI derivatives we incubated  $\beta_1$ AR with equimolar ratios of phosphatidylinositol (PI), PI(4)P, phosphatidylinositol 4,5-bisphosphate (PI(4,5)P<sub>2</sub>), and phosphatidylinositol (3,4,5)-trisphosphate (PI(3,4,5)P<sub>3</sub>) all with the same acyl chains (18:1/18:1). Plotting intensity ratio to the apo protein in the mass spectrum of each bound lipid peak against concentration showed that PI(4,5)P<sub>2</sub> bound to a greater extent than PI(4)P indicating that an additional phosphate group on PIP<sub>2</sub> increased the affinity (Fig. 1b). For PI(3,4,5)P<sub>3</sub>, in which a further phosphate group is introduced over PIP<sub>2</sub>, binding to  $\beta_1$ AR was reduced to a similar level as observed for PI, demonstrating selectivity for the PIP<sub>2</sub> head group. Analogous experiments were carried out for NTSR1 and A<sub>2A</sub>AR and in all cases (PI(4,5)P<sub>2</sub>) was found to bind with the highest affinity (Extended Data Fig. 3) implying that preferential binding sites for PIP<sub>2</sub> exist on all three class A GPCRs.

We carried out coarse-grained molecular dynamics (CGMD) simulations (Extended Data Fig. 4) to characterize the molecular nature of GPCR: PIP<sub>2</sub> interactions to the receptors in a phospholipid bilayer environment<sup>9</sup>. PIP<sub>2</sub> molecules were seen to bind at the interface formed by the cytoplasmic loops linking TM1, TM2, TM4 and TM7 of the NTSR1, with binding mediated via interactions between the triphosphorylated inositol headgroup and basic protein side chains (Fig. 1C and Extended Data Fig. 4a). Simulation of PS, also identified above, showed diffuse interaction, with lower intensity, and no obvious competition with PIP<sub>2</sub> (Extended Data Fig. 4c). Similar interactions were seen for  $\beta_1$ AR, which also exhibited the capacity for PIP<sub>2</sub> interaction with the positively charged intracellular sides of TM5-7 (Extended Data Fig. 4b). A more extensive comparison of simulations for nine Class A GPCRs (Extended Data Fig. 4d) revealed conservation of this pattern of PIP<sub>2</sub> interactions at the intracellular ends of TM helices implying a structural and/or functional significance.

To locate preferential binding sites for PIP<sub>2</sub> we performed site-directed mutagenesis on NTSR1 by changing the PIP<sub>2</sub> contact residues (Fig. 1d) to other residues that retain the expression and folded state of receptor<sup>10</sup>. We developed an MS-based strategy to analyse the impact of mutations on PIP<sub>2</sub> binding (Extended Data Fig. 5a). Mutating selected Lys/Arg residues to residues of lower mass decreased the molecular weight of the receptor, thus making the mutants “light” compared to the unmodified parental receptor (“heavy”). An equimolar solution of mutant and unmodified receptor when incubated with PIP<sub>2</sub> experiences an identical lipid environment and can be resolved by MS. Attenuation of PIP<sub>2</sub> binding was observed in TM1 (35 ± 0.03%) and TM4 (70 ± 0.13%) (Fig. 1d and Extended Data Fig. 5b) implying hotspots for PIP<sub>2</sub> binding on the cytoplasmic face of these receptors.

Given the location of these sites we reasoned that PIP<sub>2</sub> binding might influence downstream G-protein coupling. To investigate this we developed an MS approach in which the pentameric complex of A<sub>2A</sub>AR (A<sub>2A</sub>AR-mini-G $\alpha_s$ -Nb- $\beta$ - $\gamma$ )<sup>11,12</sup> was preserved in vacuum. The hetero-pentamer liberates various subcomplexes following collision-induced dissociation with (PS and PI) observed bound directly to A<sub>2A</sub>AR at higher abundance than when bound to the receptor prior to G protein coupling (Fig. 2a and Extended Data Fig. 3d). We reasoned that these lipids in receptor: triple G protein assemblies may play a role in stabilising the complex, and in turn, increase signaling. To test these effects we measured the GTPase activity of G $\alpha_i$ -G $\beta$ -G $\gamma$  when coupled to active NTSR1, stimulated by neurotensin<sub>8-13</sub>, in the presence or absence of

PIP<sub>2</sub>. We found that GTP hydrolysis was enhanced (1.3 -fold) allowing us to conclude that PIP<sub>2</sub> improves G protein coupling and GTPase activity (Fig. 2b).

Given the instability of the trimeric G protein complex it is not possible to explore the effects of lipids on coupling in an unbiased way. We therefore investigated receptor complexes formed with engineered mini-G subunits that recapitulate the increase in agonist affinity observed upon coupling with the native heterotrimeric G protein (Fig 2c). Mass spectra of thermostabilised  $\beta_1$ AR in complex with mini-G<sub>s</sub> were recorded. The association of lipids was found to be higher when  $\beta_1$ AR is in complex with mini-G<sub>s</sub> than for the receptor alone (Fig. 2d). A high population of the receptor mini-G<sub>s</sub> complex is preserved enabling the selectivity toward different subtypes of G $\alpha$  subunits (G<sub>s</sub>, G $\alpha_{i/o}$ , and G $\alpha_{12/13}$ ) to be explored. We investigated the coupling of agonist-bound  $\beta_1$ AR to mini-G<sub>i(s)</sub>, engineered from mini-G<sub>s</sub> by introducing nine mutations on the  $\alpha 5$  helix to the corresponding residues on G $\alpha_i$ , and similarly for G $\alpha_{12}$  which was prepared by transferring all the mutations from mini-G<sub>s</sub> to G<sub>12</sub><sup>2</sup>. We observed a lower extent of coupling for mini-G<sub>i(s)</sub> and virtually no coupling for mini-G<sub>12</sub> (Fig. 2d).

To investigate the effect of PIP<sub>2</sub> on GPCR: mini-G<sub>s</sub> interactions, we incubated the agonist-bound receptor  $\beta_1$ AR with the highest affinity mini-G, mini-G<sub>s</sub>, in the presence of lipid and compared the lipid-bound peaks. Although the complex can form in the absence of lipids, or with only one PIP<sub>2</sub> bound, in the presence of two or three PIP<sub>2</sub> molecules complex formation is significantly enhanced (2.7- and 4.5-fold respectively, compared to the receptor without lipid) (Fig. 3a and 3g). We also observed the same phenomenon from a time course experiment that indicated  $21 \pm 6$  % enhancement of mini-G<sub>s</sub> coupling with two PIP<sub>2</sub> molecules bound, whereas the third PIP<sub>2</sub> increases binding by an additional  $12 \pm 5$  % (Extended Data Fig. 6a).

Another anionic lipid such as PS, identified as an endogenously bound lipid to the receptor (Fig. 1A), was recruited for examining its effect on mini-G<sub>s</sub> coupling. We carried out analogous experiments using a concentration of PS 3-fold higher than that used for PIP<sub>2</sub> to reflect the reduced affinity of PS defined above (Fig. 3b and Extended Data Fig. 2). Mass spectra showed only a slight increase in the extent of mini-G<sub>s</sub> coupling as a function of PS binding. This reduced effect implies that the electrostatic interactions of the polyanionic lipid headgroups in PIP<sub>2</sub> with multiple basic sidechains, as observed in e.g. Kir channels<sup>13</sup>, are necessary for bridging receptor coupling and are not possible with PS.

Because our data imply that additional PIP<sub>2</sub>, but not PS, stabilise the complex once receptor coupling has occurred we used potential of mean force (PMF) calculations<sup>14</sup> to explore the effect of PIP<sub>2</sub> binding on the free energy landscape of A<sub>2A</sub>AR-mini-G<sub>s</sub> interactions<sup>15</sup>. Comparison of PMFs for PIP<sub>2</sub>-bound versus PS-bound receptor in a lipid bilayer indicates that the interaction of mini-G<sub>s</sub> with A<sub>2A</sub>AR is stabilised significantly ( $\sim 50 \pm 10$  kJ/mol) in the presence of PIP<sub>2</sub> compared with PS (Fig. 3c and Extended Data Fig. 6b). The presence of PIP<sub>2</sub> at the interface between the receptor and mini-G<sub>s</sub> in the PMF calculation implies that PIP<sub>2</sub> molecules form bridging interactions to stabilise the complex.

There are two potential scenarios for the increase in PIP<sub>2</sub> binding to the  $\beta_1$ AR:mini-G<sub>s</sub> complex: (i) active conformations of receptors bind more PIP<sub>2</sub> than their inactive counterparts or (ii) positively charged residues in mini-G<sub>s</sub>, at the membrane receptor-G protein interface, recruit additional PIP<sub>2</sub> molecules following

coupling. To investigate the dependence of PIP<sub>2</sub> binding on receptor conformation we incubated PIP<sub>2</sub> with  $\beta_1$ AR (co-purified with the agonist isoprenaline) and with an E130W mutation to stabilise ligand free  $\beta_1$ AR without affecting G protein coupling<sup>16</sup>. We observed a  $31 \pm 1\%$  increase in PIP<sub>2</sub> binding to the agonist-bound receptor compared to the unbound state (Extended Data Fig. 6c). While in general transition to active states is thought to involve substantial movements of TM5 and TM6, ICL2 was also found to undergo significant changes during activation of the Kappa Opioid Receptor<sup>17</sup>. Our results are consistent with PIP<sub>2</sub> stabilising active states of receptors through hotspots for binding on ICL2 directly, and diffuse intracellular PIP<sub>2</sub> binding sites more generally.

To explore scenario (ii) wherein additional PIP<sub>2</sub> binding sites form following coupling, we carried out CGMD simulations for A<sub>2A</sub>AR-mini-G<sub>s</sub>, which is the only available structure of a receptor-mini-G complex. In addition to contacts observed above, PIP<sub>2</sub> was seen to interact with the residues of mini-G<sub>s</sub> proximal to the lipid contacts on the A<sub>2A</sub>AR TM3, TM4 and TM5 interface (Fig. 3e). To investigate the significance of these additional binding sites we employed a nanobody (Nb6B9)<sup>18</sup>, where lipid binding residues observed in mini-G<sub>s</sub> are absent<sup>12</sup> (Extended Data Fig. 7). (Structures of the receptors bound to the nanobody or mini-G<sub>s</sub> are virtually identical (rms deviation 0.4-0.6 Å)<sup>19</sup>. Comparing directly the extent of PIP<sub>2</sub> binding to the receptor and receptor-nanobody complex we found that the degree of PIP<sub>2</sub> binding was closely similar (Fig. 3d and 3g). The absence of corresponding residues in the nanobody (Fig. 3e) explains the insensitivity to PIP<sub>2</sub> in receptor-nanobody complexation and implies that PIP<sub>2</sub> molecules enhance coupling via interactions specific to the receptor and mini-G<sub>s</sub>. Lipids without the polyanionic headgroups, such as PS, would not be able to induce this effect.

To investigate the possibility that specific residues on mini-G<sub>s</sub>, as opposed to other G proteins, mediate bridging we investigated the effects of PIP<sub>2</sub> on the coupling of mini-G<sub>i(s)</sub> to agonist-bound  $\beta_1$ AR. We found that coupling in the presence of PIP<sub>2</sub> was improved but to a lower extent (Fig. 3f and 3g). Given the established role in coupling to receptors of helix 5 in G $\alpha_s$  (R380), together with residues identified by MD simulation (Fig. 3e), and the fact that these residues are substituted in G $\alpha_i$  (E40, V41, K42, D216, T380) differences in PIP<sub>2</sub> binding can be attributed to disruption of these PIP<sub>2</sub> bridging sites. It follows therefore that PIP<sub>2</sub> binding sites on G $\alpha_s$ , not present on G $\alpha_i$ , enable simultaneous binding of the  $\beta_1$ AR to the G protein of highest affinity. Consequently we propose that PIP<sub>2</sub> acts as an allosteric modulator, binding to the intracellular side of the receptor, stabilising the active state and enhancing selectivity of G-protein coupling. This coupling is then further stabilised by PIP<sub>2</sub> molecules bridging between receptors and the selected G-protein.

More generally, it is established that the cytoplasmic face of GPCRs undergo conserved conformational change to allow coupling of G proteins<sup>20</sup> with the cytoplasmic ends of TM5 and TM6 moving outwards, and TM7 moving inwards slightly. Synthetic molecules that bind at the TM5-TM6-TM7 cytoplasmic interface act as negative allosteric modulators that inhibit the activation of GPCRs by preventing their movement and consequently reducing the affinity of agonists at the orthosteric binding pocket<sup>21,22</sup>. Here we highlight another role of the cytoplasmic interface through the recruitment of PIP<sub>2</sub> and the stabilisation of active G protein-bound states of GPCRs. Simultaneous binding of the PIP<sub>2</sub> head group to both the G $\alpha$

subunit and conserved TM4 residues on a number of class A receptors, that are not observed for class B receptors, suggests the generality of this mechanism for stabilising selectively active states of class A GPCRs. (Extended Data Fig. 4d and 8).

As the local concentration of PIP<sub>2</sub> in the membrane has the potential to be modulated by different signaling pathways, for example receptor tyrosine kinases or Ca<sup>2+</sup> signaling, crosstalk with GPCRs through PIP<sub>2</sub> may represent another mode of regulation in the cell<sup>23</sup>. In addition, the potential to stabilise the active conformation of G protein-coupled receptors through the binding of potent small molecules that mimic the bridging effects of the PIP<sub>2</sub> head group provides a further avenue for stabilising active states of GPCRs for therapeutic purposes. As PIP<sub>2</sub> is able to discriminate between different G protein subunits, and is likely to further distinguish binding to  $\beta$ -arrestin, there is the potential of developing novel compounds that bind specifically to different G protein-coupled or  $\beta$ -arrestin bound states, thus providing a new perspective for rational design of novel biased allosteric agonists.

## References

- 1 Hauser, A. S., Attwood, M. M., Rask-Andersen, M., Schiöth, H. B. & Gloriam, D. E. Trends in GPCR drug discovery: new agents, targets and indications. *Nat. Rev. Drug Discov.*, (2017).
- 2 Nehmé, R. *et al.* Mini-G proteins: Novel tools for studying GPCRs in their active conformation. *PLOS ONE* **12**, e0175642, (2017).
- 3 Zoher, M., Zhang, C., Rasmussen, S. G., Kobilka, B. K. & Muller, D. J. Cholesterol increases kinetic, energetic, and mechanical stability of the human beta2-adrenergic receptor. *Proc. Natl. Acad. Sci. U. S. A.* **109**, E3463-3472, (2012).
- 4 Dawaliby, R. *et al.* Allosteric regulation of G protein-coupled receptor activity by phospholipids. *Nat. Chem. Biol.* **12**, 35-39, (2016).
- 5 Gault, J. *et al.* High-resolution mass spectrometry of small molecules bound to membrane proteins. *Nat. Methods* **13**, 333-336, (2016).
- 6 Yen, H. Y. *et al.* Ligand binding to a G protein-coupled receptor captured in a mass spectrometer. *Sci. Adv.* **3**, e1701016, (2017).
- 7 Egloff, P. *et al.* Structure of signaling-competent neurotensin receptor 1 obtained by directed evolution in *Escherichia coli*. *Proc. Natl. Acad. Sci. U. S. A.* **111**, E655-662, (2014).
- 8 Inagaki, S., Ghirlardo, R. & Grisshammer, R. Biophysical characterization of membrane proteins in nanodiscs. *Methods* **59**, 287-300 (2013).
- 9 Hedger, G. & Sansom, M. S. P. Lipid interaction sites on channels, transporters and receptors: Recent insights from molecular dynamics simulations. *Biochimica et Biophysica Acta-Biomembranes* **1858**, 2390-2400, (2016).
- 10 Schlinkmann, K. M. *et al.* Critical features for biosynthesis, stability, and functionality of a G protein-coupled receptor uncovered by all-versus-all mutations. *Proc. Natl. Acad. Sci. U. S. A.* **109**, 9810-9815, (2012).
- 11 Carpenter, B., Nehmé, R., Warne, T., Leslie, A. G. W. & Tate, C. G. Structure of the adenosine A2A receptor bound to an engineered G protein. *Nature* **536**, 104-107, (2016).
- 12 Rasmussen, S. G. *et al.* Structure of a nanobody-stabilized active state of the beta(2) adrenoceptor. *Nature* **469**, 175-180, (2011).
- 13 Hansen, S. B., Tao, X. & MacKinnon, R. Structural basis of PIP(2) activation of the classical inward rectifier K(+) channel Kir2.2. *Nature* **477**, 495-498, (2011).
- 14 Roux, B. The calculation of the potential of mean force using computer simulations. *Comput. Phys. Commun.* **91**, 275-282 (1995).
- 15 Domański, J., Hedger, G., Best, R. B., Stansfeld, P. J. & Sansom, M. S. P. Convergence and Sampling in Determining Free Energy Landscapes for Membrane Protein Association. *J. Phys. Chem. B* **121**, 3364-3375, (2017).
- 16 Roth, C. B., Hanson, M. A. & Stevens, R. C. Stabilization of the  $\beta$ 2-adrenergic Receptor 4-3-5 Helix Interface by Mutagenesis of Glu-122(3.41), A Critical Residue in GPCR Structure. *J. mol. biol.* **376**, 1305-1319, (2008).
- 17 Che, T. *et al.* Structure of the Nanobody-Stabilized Active State of the Kappa Opioid Receptor. *Cell* **172**, 55-67 e15, (2018).

- 18 Miller-Gallacher, J. L. *et al.* The 2.1 Å resolution structure of cyanopindolol-bound beta1-adrenoceptor identifies an intramembrane Na<sup>+</sup> ion that stabilises the ligand-free receptor. *PLoS One* **9**, e92727, (2014).
- 19 Injin, B. & Hee-Jung, C. Structural Features of  $\beta_2$  Adrenergic Receptor: Crystal Structures and Beyond. *Mol. Cells* **38**, 105-111 (2015).
- 20 Venkatakrisnan, A. J. *et al.* Diverse activation pathways in class A GPCRs converge near the G-protein-coupling region. *Nature* **536**, 484-487, (2016).
- 21 Zheng, Y. *et al.* Structure of CC chemokine receptor 2 with orthosteric and allosteric antagonists. *Nature* **540**, 458-461, (2016).
- 22 Liu, X. *et al.* Mechanism of intracellular allosteric beta2AR antagonist revealed by X-ray crystal structure. *Nature* **548**, 480-484, (2017).
- 23 Gavi, S., Shumay, E., Wang, H. Y. & Malbon, C. C. G-protein-coupled receptors and tyrosine kinases: crossroads in cell signaling and regulation. *Trends Endocrinol Metab* **17**, 48-54, (2006).

## Acknowledgments

CVR acknowledges an ERC Advanced Grant ENABLE (641317), an MRC Programme Grant (G1000819) and a Wellcome Trust Investigator Award (104633/Z/14/Z). Further support was provided by the MRC (GH), the Royal Society Newton International Fellowship (WS), and the BBSRC (MSPS; BB/L002558/1) and the Wellcome Trust (MSPS; 092970/Z/10/Z). This work used the ARCHER UK National Supercomputing Service (<http://www.archer.ac.uk>) supported by EPSRC. AP was funded by the Schweizerischer Nationalfonds Grant (31003A\_153143). CGT acknowledges the MRC (MC\_U105197215), an ERC Advanced Grant EMPSI (339995) and funding from Heptares Therapeutics. We thank Matthias Hillenbrand for kindly providing SF9 cells.

## Author contributions

H.-Y.Y., K.H.K. and I.L. performed all the mass spectrometry experiments on the GPCR, mini-G<sub>s</sub> and nanobody. D.W. performed lipidomics. G.H., M.R.H., W.S., and M.S.P.S. performed MD simulations and analysis. P.H. purified the NTSR1 receptor in the apo-state. T.W. purified  $\beta_1$ AR, Y.L. purified A<sub>2A</sub>R and B.C. purified mini-G<sub>s</sub>. A.P., C.G.T., M.S.P.S. and C.V.R supervised the research and H.-Y.Y. and C.V.R. wrote the paper with contributions from all authors.

## Author information

Reprints and permissions information is available at [www.nature.com/reprints](http://www.nature.com/reprints). The authors declare competing interests: H.-Y.Y., and I.L. are founders and employees of OMass Technologies. C.V.R is a founder and consultant of OMass Technologies. Correspondence and requests for materials should be addressed to C.V.R ([carol.robinson@chem.ox.ac.uk](mailto:carol.robinson@chem.ox.ac.uk)).

## Online Methods

### Constructs and proteins

Expression plasmids for two rat NTSR1 stabilised variants<sup>7,24</sup> were used in our experiments. NTSR1 HTGH4- $\Delta$ IC3B contains the protein sequence from amino acid 50 to 390 with an ICL3 deletion (273-290) and 26 thermostabilising point mutations. It should be noted that this construct is only 80% identical to the wild-type. NTSR1 HTGH4 43-421 contains the intact protein sequence from 43-421, with the same stabilising mutations. Purified thermostabilised turkey (*M. gallopavo*)  $\beta_1$ AR, human wild-type  $A_{2A}$ R, engineered  $G\alpha_s$  (mini- $G_s$ ) and Nanobody Nb6B9 were utilized for mass spectrometry analysis<sup>11,25,26</sup>. The following thermostabilising point mutations on  $\beta_1$ AR were used throughout: R68S, M90V, F327A, F338M (for stabilising), C116L (to increase protein expression), R284K (residue equivalent to  $\beta_2$ AR designed to improve Nb80 binding), C358A (prevention of potential palmitoylation). In order to purify receptor in the unliganded state, the construct with the same thermostabilising mutations but slightly different lengths of TM1 was introduced with an additional mutation (E130W) for stabilising the receptor. The use of an N-terminal TrxA fusion (C32S & C35S) on the receptor was necessary to confirm formation of a complex on SDS gels. The insect cell lines (Sf9 and Tni) were obtained from Invitrogen and examined without mycoplasma contamination.

### Protein expression and purification

#### Expression and purification of $\beta_1$ AR.

The turkey (*M. gallopavo*)  $\beta_1$ AR constructs used ( $\beta_118$  and  $\beta_114$ -E130W) were based on the previously published thermostabilised  $\beta_1$ AR44-m23 construct but contained only four (R68S, M90V, F327A, F338M) of the original six thermostabilising mutations, as the two mutations on transmembrane helices 5 and 6 (Y227A and A282L) were not included. The omission of these two mutations resulted in constructs that demonstrated coupling to G proteins and to G protein mimetic nanobody Nb80 along with high affinity agonist binding<sup>25</sup>. The constructs included Thioredoxin (*E. coli*) fused to the N-terminus of transmembrane helix 1 and the mutations C116L to improve expression and C358A to prevent potential palmitoylation. Both constructs were expressed in insect cells using recombinant baculoviruses prepared using the transfer vector pAcGP67B (BD Biosciences) and BacPAK6 linearized baculovirus DNA (Oxford Expression Technologies). The membrane containing the expressed receptor was solubilized and purified in 2% and 0.02% dodecylmaltoside (DDM, Generson), respectively, as described previously<sup>27-29</sup>. For  $\beta_118$ , the final purification step was competitive elution from an alprenolol sepharose ligand affinity column in 20mM Tris-HCl, pH7.4, 350 mM NaCl and 0.02% DDM supplemented with 1mM isoprenaline so that the receptor was prepared with agonist ligand bound. The purified receptor was finally concentrated to 15mg/ml in the alprenolol sepharose elution buffer.

$\beta_114$ -E130W contained the mutation E130W that increased functional expression of  $\beta_1$ AR<sup>16</sup>. The use of this mutation facilitated the preparation of highly purified active receptor without any ligand bound as the use of a ligand affinity chromatography step was not necessary to separate non-functional receptor. For  $\beta_114$ -E130W purification in 0.02% DDM was by  $Ni^{2+}$  affinity chromatography followed by a thrombin (Sigma) protease cleavage step to remove the His tag before further purification by SEC on a Superdex Increase 200 10/300GL column (GE Healthcare) in 20mM Tris-HCl, pH7.4, 100 mM NaCl and 0.02% DDM, with final concentration to 45mg/ml.

#### Expression and purification of adenosine $A_{2A}$ R.

The human adenosine  $A_{2A}$ R construct used (residues 1–308) was modified with a C-terminal histidine tag (His10) preceded by a TEV protease cleavage site, and by the mutation N154A to prevent N-linked glycosylation. The  $A_{2A}$ R was expressed in insect cells using the baculovirus system, insect cell membranes were prepared and solubilised with 2% lauryl maltose neopentyl glycol (LMNG, Anatrace) and the receptor purified by  $Ni^{2+}$  affinity chromatography and size-exclusion chromatography (SEC), utilizing a Superdex Increase 200 10/300GL column (GE) run in 20 mM HEPES pH 7.5, 100 mM NaCl, 10% (v/v) glycerol, 0.01% (w/v) LMNG and concentrated to 10mg/ml. Purification was as described previously<sup>11</sup>, with the exception that the receptor was purified without addition of ligand.

#### Expression and purification of mini- $G_s$ , mini- $G_i$ and mini- $G_{12}$

The engineered minimal G proteins, mini- $G_s$  construct R414<sup>25</sup>, mini- $G_i$  construct and mini- $G_{12}$  construct 8<sup>2</sup> were expressed in *E. coli* and purified by  $Ni^{2+}$  affinity chromatography, followed by cleavage of the histidine tag using TEV protease and negative purification on  $Ni^{2+}$ -NTA to remove TEV and undigested mini-G protein, and finally SEC to remove aggregated protein as described

elsewhere<sup>25,30</sup>, with final concentration up to 100 mg/ml in 10 mM HEPES, pH 7.5, 100 mM NaCl, 10% v/v glycerol, 1 mM MgCl<sub>2</sub>, 1 μM GDP and 0.1 mM TCEP.

#### **Expression and purification of nanobody Nb6B9.**

A synthetic gene (Integrated DNA Technologies) for Nb6B9<sup>12,31</sup> was cloned into the plasmid pET-26b(+) (Novagen) with a N-terminal His6 tag followed by a thrombin protease cleavage site.

Expression was in *E. coli* strain BL21(DE3)RIL (Agilent Technologies) and purification from the periplasmic fraction was by Ni<sup>2+</sup> affinity chromatography, but with the use of a thrombin (Sigma) protease cleavage step to remove the His tag before concentration to 40 mg/ml.

#### **Preparation of receptor G protein complexes.**

Several receptor-G protein complexes were made for MS analysis; A<sub>2A</sub>R-mini-Gsβγ, which is prepared by incubating A<sub>2A</sub>R, with a TrxA fusion at the N-terminal, co-purified with NECA and the trimeric G proteins consisted of mini-G<sub>s</sub>, Gβ and Gγ in the presence of nanobody Nb35 at 1:2:4 molar ratio (Receptor:G proteins:Nb) to stabilise the complex. The complex was further purified by gel-filtration chromatography after overnight incubation. β<sub>1</sub>AR-miniG, which is prepared by incubating β<sub>1</sub>AR co-purified with isoprenaline and different subtypes of mini-G protein (mini-G<sub>s</sub>, mini-G<sub>i(s)</sub> and mini-G<sub>12</sub>) at 1:1.2 molar ratio. The incubation time is varied in order to capture the equilibrium of complex formation.

#### **Purification of heterotrimeric G protein.**

Baculovirus encoding the desired subunits (α<sub>i1</sub>β<sub>1</sub>γ<sub>1</sub>) were used to express the heterotrimeric G protein in Sf9 cells as previously described<sup>32</sup>. The cells from 1L expression culture were resuspended and lysed in lysis buffer (10 mM HEPES pH 7, 20 mM KCl, 10 mM MgCl<sub>2</sub>, 10 μM GDP, 2 mM β-mercaptoethanol, and cOmplete protease inhibitor (Roche)). The membranes were pelleted by ultracentrifugation at 108,000 × g for 35 min and solubilized in solubilisation buffer (50 mM HEPES pH 7, 150 mM NaCl, 10 mM MgCl<sub>2</sub>, 10 μM GDP, 2 mM β-mercaptoethanol, 1% decyl-β-D-maltopyranoside (DM) (w/v), 10% (v/v) glycerol, and cOmplete protease inhibitor (Roche)) for 3 h. The supernatant was collected after centrifugation at 108,000 × g for 35 min and incubated with 1.2 mL of TALON beads (GE Healthcare) overnight. The beads were collected and washed by ten column volumes (CV) of wash buffer (30 mM HEPES pH 7, 300 mM NaCl, 10 mM MgCl<sub>2</sub>, 25 mM Imidazole pH 8, 10 μM GDP, 2 mM β-mercaptoethanol, 10% (v/v) glycerol, and 0.5% (w/v) DM), followed by another twenty CV wash of wash buffer containing 40 mM Imidazole (pH 8.0) and were eluted with five CV elution buffer (30 mM HEPES pH 7, 150 mM NaCl, 1 mM MgCl<sub>2</sub>, 300 mM Imidazole pH 8, 10 μM GDP, 2 mM β-mercaptoethanol, 10% (v/v) glycerol, and 0.5% (w/v) DM). The protein was further purified by a Superdex 200 Increase PC 3.2/300 column (GE Healthcare) and the protein tag was removed by incubation with human rhinovirus 3C protease (in-house produced) overnight. Following the buffer exchange to storage buffer (20 mM HEPES pH 7, 100 mM NaCl, 0.1 mM MgCl<sub>2</sub>, 4 mM β-mercaptoethanol, 10% (v/v) glycerol, and 0.5% (w/v) DM) and reverse IMAC by Ni-NTA superflow beads (GE Healthcare), G protein complex was concentrated to at least 2 mg/mL for experimental use.

**NTSRI expression:** *E. coli* BL21 cells were transformed with the expression plasmid encoding NTSRI HTGH4-ΔIC3B and grown overnight at 37°C in 20 ml of 2YT medium supplemented with 1% (w/v) glucose and 100 μg/ml ampicillin. Two shake flasks containing each 1 L of 2YT medium, 0.5% (w/v) glucose, and 100 μg/ml ampicillin were inoculated using 10 ml pre-culture and grown to an OD<sub>600</sub> of 0.5 at 37°C. Receptor expression was induced with 1 mM isopropyl-β-D-thiogalactopyranoside (IPTG) and cells were cultivated at 28°C overnight. Cells were harvested after overnight expression and *E. coli* cell pellets were resuspended in 100 ml of solubilisation buffer, containing 100 mM HEPES pH 8.0, 20% (v/v) glycerol and 400 mM NaCl. Resuspended cells were frozen in liquid nitrogen and stored at -80 °C.

**NTSRI apo purification:** The cell pellet was thawed at room temperature. All following steps were carried out at 4 °C. 0.5 mL of 1 M MgCl<sub>2</sub> (5 mM), 2 mg DNase I, 200 mg lysozyme, and 20 ml of a detergent mixture (composed of 0.2% (w/v) cholesteryl hemisuccinate Tris salt (CHS) and 2% (w/v) dodecyl-β-D-maltopyranoside (DDM)) were added to the thawed cell pellet. The mixture was incubated for 1 h, followed by cell lysis via mild sonication for 30 min in an ice-water bath. After cell lysis, 0.4 ml of 5 M imidazole was added and the mixture was incubated for another 30 min. The suspension was centrifuged for 30 min at 28,000 × g. The supernatant was mixed with 5 ml of TALON resin (Clontech, Mountain View, CA, USA), which had been pre-equilibrated with IMAC binding

buffer (25 mM HEPES pH 8.0, 10% (v/v) glycerol, 600 mM NaCl, 0.1% (w/v) DDM and 20 mM imidazole) and incubated overnight on a rolling device. The mixture was loaded into a PD10 column (GE Healthcare, Uppsala, Sweden) and was washed with 50 ml of IMAC binding buffer. Elution of bound protein was performed with 15 ml IMAC elution buffer containing 25 mM Hepes pH 8.0, 10% (v/v) glycerol, 150 mM NaCl, 0.1% (w/v) DDM and 250 mM imidazole. Eluted receptor was concentrated in an Amicon-15 Ultra concentrator with a 100 kDa cut-off (Millipore, Billerica, MA, USA) to a final volume of less than 2.5 ml. Concentrated receptor sample was loaded on a Sephadex G-25 desalting column (GE Healthcare, Uppsala, Sweden), pre-equilibrated with 25 mM Hepes pH 8.0, 10% (v/v) glycerol, 150 mM NaCl, 0.1% (w/v) DDM to remove remaining imidazole. Desalted receptor was incubated with 300  $\mu$ l of 1.6 mg/ml HRV 3C protease for 1 h at 4°C, followed by addition of 150  $\mu$ l 10% (w/v) LMNG and incubation for 1 h at 4°C. The cleaved protein was diluted threefold with reverse IMAC buffer (10 mM HEPES pH 8.0, 10% (v/v) glycerol, 150 mM NaCl, and 0.01% (w/v) LMNG) and was loaded onto a PD10 column containing 5 ml Ni-NTA beads pre-equilibrated with reverse IMAC buffer. The flow-through was collected in an Amicon-15 ultra concentrator with a 50 kDa cut-off and the resin was further washed with 10 ml buffer. Receptor was concentrated to a final volume of less than 1 ml and was subjected to preparative size exclusion chromatography using a Superdex 200 10/300 GL column (GE Healthcare, Uppsala, Sweden), which had been pre-equilibrated with 10 mM HEPES pH 8, 150 mM NaCl, and 0.01% (w/v) LMNG. Peak fractions corresponding to NTSR1 HTGH4- $\Delta$ IC3B were pooled (final volume 3-4 ml) and concentrated in an Amicon-4 ultra-concentrator with a 50 kDa cut-off to a final protein concentration of approximately 50  $\mu$ M. Purified and concentrated NTSR1-H4 was mixed with 10 mM HEPES pH 8, 150 mM NaCl, 0.01% (w/v) LMNG, and 50% (v/v) glycerol to yield a final glycerol concentration of 25%. Aliquots were frozen in liquid nitrogen and stored at -80 °C for later usage.

### Preparation of phospholipids and titration experiment

Phospholipids were purchased from Avanti (Avanti Polar Lipids Inc., Alabama, USA) and prepared as stock concentration of 3 mM in 200 mM ammonium acetate buffer pH 7.5 containing the detergent mixed micelle preparation, which contains DDM and foscholine as previously described<sup>33</sup>. A phosphate analysis was performed to determine the concentration of phospholipids in solution<sup>34</sup>. For the titration experiment, 5  $\mu$ M of buffer exchanged receptors in 200 mM ammonium acetate buffer pH 7.5 containing the detergent mixtures (DDM, LMNG, and foscholine for NTSR1; DDM and foscholine for  $\beta_1$ AR and A<sub>2A</sub>R) were mixed with lipids at various concentration points followed by equilibration at 4 °C for 5 min, by which time lipid binding had stabilised according to our time course measurements. Following mass spectrometry analysis UniDec (Universal Deconvolution) software was utilized to quantify the relative abundance of each lipid bound state<sup>35</sup>, and statistical analysis was performed by GraphPad Prism assuming a one-site total binding model.

### Lipidomics analysis

Co-purified lipids from recombinant GPCRs were extracted by chloroform/methanol (2:1, v/v) and lyophilized and re-dissolved in 60% acetonitrile (ACN). For LC-MS/MS analysis, the extracted lipids were separated on a C18 column (Acclaim PepMap 100, C18, 75 mm  $\times$  15 cm; Thermo Scientific) by means of Dionex UltiMate 3000 RSLC nano LC System. The buffers and gradient are adapted from a previous protocol.<sup>36</sup> Briefly, the lipids were separated using a binary buffer system at 40°C using a gradient of 32% to 99% buffer B at a flow rate of 300 nl/min over 30 min. (Buffer A: (ACN: H<sub>2</sub>O (60:40), 10 mM ammonium formate, 0.1% formic acid) and buffer B (IPA: ACN (90:10), 10 mM ammonium formate, 0.1% formic acid)). The column eluent was delivered via a dynamic nanospray source to a hybrid LTQ Orbitrap mass spectrometer (Thermo Scientific). Typical MS conditions were: spray voltage (1.8 kV) and capillary temperature (175 °C). The LTQ-Orbitrap XL was operated in negative ion mode and in data-dependent acquisition with one MS scan followed by five MS/MS scans<sup>37</sup>. Survey full-scan MS spectra were acquired in the orbitrap (m/z 350 – 2,000) with a resolution of 60,000. Collision-induced dissociation (CID) fragmentation in the linear ion trap was performed for the five most intense ions at an automatic gain control target of 30,000 and a normalized collision energy of 38% at an activation of q = 0.25 and an activation time of 30 ms.

### GTPase assay

The GTPase activity of trimeric G $\alpha_i\beta\gamma$  was measured by using a commercial GTPase-Glo™ assay (Promega). The assay was performed in white 384-well plates (Corning) using purified trimeric G proteins diluted into a GTPase buffer (10 mM HEPES pH 7, 50 mM NaCl, 0.05 mM MgCl<sub>2</sub>, 2 mM  $\beta$ -mercaptoethanol, 1mM DTT, 5 % (v/v) glycerol, and 0.25% (w/v) DM) at a final concentration 2.5

$\mu\text{M}$  in the presence of 5  $\mu\text{M}$  GTP. The luminescent signal was measured after incubation at room temperature (1 h) following the protocol provided to indicate the level of residual GTP. To analyse the impact of  $\text{PIP}_2$  we used NTSR1 HTGH4- $\Delta\text{IC3B}$  co-purified with recombinant neurotensin<sub>8-13</sub> following the method described previously<sup>38</sup>. The receptor was pre-incubated with detergent solubilised  $\text{PIP}_2$  at 1:3 molar ratio (receptor to lipid) in the protein buffer (10 mM HEPES pH 8, 150 mM NaCl, 0.01% (w/v) LMNG) containing 100 nM neurotensin<sub>8-13</sub> for 15 min on ice. The activated receptor was then added to the reaction mixture containing trimeric G proteins under the condition described above.

### **Native mass spectrometry of GPCRs**

Purified GPCRs were buffer exchanged into 200 mM ammonium acetate buffer pH 7.5 containing the mixed micelle preparation optimized for GPCR analysis as described previously<sup>6</sup>. The concentration of DDM, foscholine and CHS required to form a mixed micelle range from 0.006-0.02%, 0-0.002%, and 0.001-0.01%, respectively and are optimized for each receptor preparation. The samples were immediately introduced into a modified Q-Exactive mass spectrometer (Thermo) described previously<sup>5</sup>. Ions were transferred into the Higher-energy collisional dissociation (HCD) cell following a gentle voltage gradient (injection flatapole, inter-flatapole lens, bent flatapole, transfer multipole: 7.9, 6.94, 5.9, 4 V respectively). An optimized acceleration voltage (100-130 V) was then applied to the HCD cell to remove the detergent micelle from the protein ions. Backing pressure was maintained at  $\sim 1.00 \times 10^{-9}$  mbar and data was analysed using Xcalibur 2.2 SP1.48.

The bound lipid identification experiments were performed with a modified Synapt G2 mass spectrometer (Waters) equipped with a Z-spray source<sup>33,39</sup>. The typical instrumental setting was source pressure (4.5-5 mbar) capillary voltage (1.2 – 1.5 kV) and cone voltage (100–200V). An extraction voltage of 1-5 V was applied and 80–150V was used as the collision voltage with argon as the collision gas at a pressure of 0.2–0.3 MPa. To strip the detergent from protein ions in the source region, instrument values were optimized to capillary voltage (1.5 kV), cone voltage (200 V) and extraction voltage (3 V). A collision voltage ramp (from 20 – 100 V) was applied to dissociate protein-lipid complexes after quadrupole selection.

### **Identification of preferential $\text{PIP}_2$ binding sites on NTSR1**

Unmodified NTSR1 and NTSR1 variants were pre-incubated at 1:1 molar ratio to give a total protein concentration of 12 mM in the protein buffer (10 mM HEPES pH 8, 150 mM NaCl, 0.01% (w/v) LMNG and 25% (v/v) glycerol). Detergent solubilised  $\text{PI}(4,5)\text{P}_2$  was then added to the protein mixture at final molar ratio of 1.25:1 lipid:receptor. The reaction mixture was incubated at 4 °C for 5 min and analysed by MS after buffer exchanging to 200 mM ammonium acetate buffer containing the mix of detergents of DDM, LMNG and foscholine as described previously<sup>6</sup>.

The ratio of  $\text{PIP}_2$  binding to the receptor was calculated by normalizing the intensity of the receptor in  $\text{PIP}_2$  bound states to the unbound state using UniDec software. The results were evaluated by comparing the ratio of  $\text{PIP}_2$  binding between mutants and the unmodified receptor and plotted as a bar chart using GraphPad Prism.

### **Mini-Gs and nanobody coupling to $\beta_1\text{AR}$**

Effector coupling to  $\beta_1\text{AR}$  was analysed by a modified Q-Exactive mass spectrometer after incubating purified  $\beta_1\text{AR}$  with mini-G<sub>s</sub>/Nb6B9 at 1:1.2 molar ratio at 4 °C in the protein buffer (20mM Tris-HCl, pH7.4, 350 mM NaCl and 0.02% DDM). The relative percentage of effector coupling was quantified by UniDec software. A time course was performed with aliquots sampled after 2, 10, 30, and 60 min to monitor the formation of the mini-G<sub>s</sub>-receptor complex. To investigate the effect of  $\text{PIP}_2$  on coupling,  $\beta_1\text{AR}$  was pre-incubated with detergent solubilised  $\text{PIP}_2$  at 1:1 molar ratio for 5 min at 4 °C to equilibrate before mixing with mini-G<sub>s</sub> or Nb6B9 at 1.2 or 0.3 molar ratio to receptor, respectively. For the analogous PS binding experiment we pre-incubated  $\beta_1\text{AR}$  with a 3-fold higher concentration of detergent solubilised PS than  $\text{PIP}_2$  (PS:  $\beta_1\text{AR}$  3:1 molar ratio) for 5 min at 4°C to equilibrate before mixing with mini-G<sub>s</sub>.

### **Modelling and simulation system setup**

Simulations were performed using the GROMACS v4.6.3 simulation package<sup>1</sup>. Initial protein coordinates were obtained using 4BUO (NTSR1) and 2Y03 ( $\beta_1\text{AR}$ ), with missing atoms added using MODELLER<sup>40</sup>. In the case of  $\beta_1\text{AR}$ , a model was also constructed in which S68 in the thermostabilised structure 2Y03 was back-mutated to R68 to reconstruct available basic residues in the wild-type receptor by using the mutagenesis tool implemented in PyMOL (Schrodinger, L.L.C. The

PyMOL Molecular Graphics System, Version 1.3r1 (2010)). Side chain ionisation states were modelled using pdb2gmx<sup>41</sup>. The N and C-termini were treated with neutral charge. Each protein structure was then energy minimized using the steepest descents algorithm implemented in GROMACS, before being converted to a coarse-grained (CG) representation using the MARTINI 2.2 force field<sup>42</sup>. The energy minimized CG structure was centered in a periodic simulation box with dimensions 11 x 11 x 12 nm<sup>3</sup>. 1-palmitoyl-2-oleoyl-sn-glycero-3-phosphocholine (POPC) molecules were randomly placed around the protein and the system solvated and neutralised to a concentration of 0.15 M NaCl. An initial 50 ns of coarse-grained simulation was applied to permit the self-assembly of a POPC lipid bilayer around the GPCR. POPC lipids were randomly exchanged<sup>43</sup> to create a mixed-species bilayer of specified composition (Extended Data Table 2). A cut-off distance of 2.5 nm was applied, with only molecules outside this distance being subject to exchange. The exchange protocol was conducted independently for each repeat simulation, such that different random initial configurations of lipids around the protein were generated for each simulation repeat. A summary of simulations performed is provided in Extended Data Table 2.

### Simulation details

The MARTINI force field<sup>42</sup> was used to describe all system components. An ELNEDYN network<sup>44</sup> was applied to the protein using a force constant of 500 kJ/mol/nm<sup>2</sup> and a cut off of 1.5 nm. Simulations were performed as an NPT ensemble, with temperature maintained at 310 K using a Berendsen thermostat<sup>45</sup> using a coupling constant of  $\tau_t = 4$  ps, and semi-isotropic pressure controlled at 1 bar using a Berendsen barostat<sup>45</sup> with a coupling constant of  $\tau_p = 4$  ps and a compressibility of  $5 \times 10^{-6}$  bar<sup>-1</sup>. Electrostatics were modeled using the reaction field coulomb type<sup>46</sup>, and smoothly shifted between 0 and 1.2 nm. Van der Waals interactions were treated using a shifting function between 0.9 and 1.2 nm. Covalent bonds were constrained to their equilibrium values using the LINCS algorithm<sup>47</sup>. Equations of motion were integrated utilizing the leap-frog algorithm, with a 20 fs time step. All simulations were run in the presence of conventional MARTINI water, and neutralised to a concentration of 0.15 M NaCl.

Analysis of simulation data was conducted using VMD<sup>48</sup>, PyMOL (Schrodinger, L.L.C. The PyMOL Molecular Graphics System, Version 1.3r1 (2010)), and tools implemented in GROMACS<sup>41</sup>, and in-house protocols. Protein-lipid contact analysis employed a cut-off distance of 0.6 nm, based on radial distribution functions for CG lipid molecules<sup>49</sup>.

### A<sub>2A</sub>R-mini-G<sub>s</sub> PMF calculations

PMFs for the interaction of mini-G<sub>s</sub> with A<sub>2A</sub>R in a lipid bilayer the presence and absence of PIP<sub>2</sub> were calculated using the MARTINI force field<sup>50</sup>. To obtain a PIP<sub>2</sub>-bound A<sub>2A</sub>R-mini-G<sub>s</sub> complex, we first ran ten coarse-grained MD simulations on receptor embedded in an asymmetric complex membrane, each lasting 8  $\mu$ s (Extended Data Table 2). The Root Mean Square Displacement (RMSD) to the crystal structure of A<sub>2A</sub>R-mini-G<sub>s</sub> complex (PDB 5G53) was calculated for the protein in these ten simulations, and the protein complex with the lowest RMSD was saved together with the membrane bilayer. The coarse grained mini-G<sub>s</sub> was then docked back to the membrane-embedded receptor based on the A<sub>2A</sub>R-mini G<sub>s</sub> crystal structure to generate the starting configuration of a steered MD (SMD) simulation. In the SMD, the mini-G<sub>s</sub> was pulled away from the receptor along z axis (normal to the membrane plane) at a rate of 0.05 nm/ns using a force constant of 1000 kJ/mol/nm<sup>2</sup> while the receptor was restrained in place using a harmonic force of 1000 kJ/mol/nm<sup>2</sup>. The distance between the center of mass (COMs) of the receptor and the mini-G<sub>s</sub> was defined as the 1D reaction coordinate and the pulling process covered a distance of 3 nm. The initial configurations of the umbrella sampling were extracted from the SMD trajectory spacing 0.05 nm apart along the reaction coordinate. 50 umbrella sampling windows were generated, and each was subjected to 1  $\mu$ s MD simulation, in which a harmonic restrain of 1000 kJ/mol/nm<sup>2</sup> was imposed on the distance between the COMs of the receptor and the mini-G<sub>s</sub> to maintain the separation of the two. The PMF was extracted from the umbrella sampling using the Weighted Histogram Analysis Method (WHAM) provided by the GROMACS g\_wham tool<sup>51</sup>. A Bayesian bootstrap was used to estimate the statistical error of the energy profile. The PMF of the binding process in the absence of PIP<sub>2</sub> was calculated following the same protocol, with the only change made to the lipid composition of the membrane lower leaflet. PIP<sub>2</sub> was taken out from the membrane and instead the concentrations of POPC, DOPC, POPE and DOPE were increased by 2.5% to make up for the vacancy left by the absence of PIP<sub>2</sub>.

### Data availability

All relevant data are available from corresponding authors on request.

- 24 Scott, D. J., Kummer, L., Egloff, P., Bathgate, R. A. D. & Plückthun, A. Improving the apo-state detergent stability of NTS1 with CRESS for pharmacological and structural studies. *Biochimica et Biophysica Acta- Biomembranes* **1838**, 2817-2824, (2014).
- 25 Carpenter, B. & Tate, C. G. Engineering a minimal G protein to facilitate crystallisation of G protein-coupled receptors in their active conformation. *Protein Eng. Des. Sel.* **29**, 583-594, (2016).
- 26 Warne, T. *et al.* Structure of a beta1-adrenergic G-protein-coupled receptor. *Nature* **454**, 486-491, (2008).
- 27 Warne, T., Serrano-Vega, M. J., Tate, C. G. & Schertler, G. F. Development and crystallization of a minimal thermostabilised G protein-coupled receptor. *Protein Expr. Purif.* **65**, 204-213 (2009).
- 28 Warne, T., Chirnside, J. & Schertler, G. F. Expression and purification of truncated, non-glycosylated turkey beta-adrenergic receptors for crystallization. *Biochim. Biophys. Acta.* **1610**, 133-140 (2003).
- 29 Warne, T. *et al.* The structural basis for agonist and partial agonist action on a beta(1)-adrenergic receptor. *Nature* **469**, 241-244, (2011).
- 30 Carpenter, B. & Tate, C. G. Expression and Purification of Mini G Proteins from Escherichia coli. *Bio Protoc.* **7**, (2017).
- 31 Ring, A. M. *et al.* Adrenaline-activated structure of beta2-adrenoceptor stabilized by an engineered nanobody. *Nature* **502**, 575-579, (2013).
- 32 Hillenbrand, M., Schori, C., Schoppe, J. & Pluckthun, A. Comprehensive analysis of heterotrimeric G-protein complex diversity and their interactions with GPCRs in solution. *Proc. Natl. Acad. Sci. U. S. A.* **112**, E1181-1190, (2015).
- 33 Laganowsky, A., Reading, E., Hopper, J. T. S. & Robinson, C. V. Mass spectrometry of intact membrane protein complexes. *Nat. Protocols* **8**, 639-651, (2013).
- 34 Chen, P. S., Toribara, T. Y. & Warner, H. Microdetermination of Phosphorus. *Anal. Chem.* **28**, 1756-1758, (1956).
- 35 Marty, M. T. *et al.* Bayesian deconvolution of mass and ion mobility spectra: from binary interactions to polydisperse ensembles. *Anal. Chem.* **87**, 4370-4376, (2015).
- 36 Bird, S. S., Marur, V. R., Sniatynski, M. J., Greenberg, H. K. & Kristal, B. S. Lipidomics Profiling by High Resolution LC-MS and HCD Fragmentation: Focus on Characterization of Mitochondrial Cardiolipins and Monolysocardiolipins. *Anal. Chem.* **83**, 940-949, (2011).
- 37 Bechara, C. *et al.* A subset of annular lipids is linked to the flippase activity of an ABC transporter. *Nat. Chem.* **7**, 255-262, (2015).
- 38 Egloff, P., Deluigi, M., Heine, P., Balada, S. & Pluckthun, A. A cleavable ligand column for the rapid isolation of large quantities of homogeneous and functional neurotensin receptor 1 variants from E. coli. *Protein Expr. Purif.* **108**, 106-114, (2015).
- 39 Sobott, F., Hernández, H., McCammon, M. G., Tito, M. A. & Robinson, C. V. A Tandem Mass Spectrometer for Improved Transmission and Analysis of Large Macromolecular Assemblies. *Anal. Chem.* **74**, 1402-1407, (2002).
- 40 Šali, A. & Blundell, T. L. Comparative Protein Modelling by Satisfaction of Spatial Restraints. *J. mol. biol.* **234**, 779-815, (1993).
- 41 Hess, B., Kutzner, C., van der Spoel, D. & Lindahl, E. GROMACS 4: Algorithms for Highly Efficient, Load-Balanced, and Scalable Molecular Simulation. *J. Chem. Theory Comput.* **4**, 435-447, (2008).
- 42 de Jong, D. H. *et al.* Improved Parameters for the Martini Coarse-Grained Protein Force Field. *J. Chem. Theory Comput.* **9**, 687-697, (2013).
- 43 Koldsø, H., Shorthouse, D., Hélie, J. & Sansom, M. S. P. Lipid Clustering Correlates with Membrane Curvature as Revealed by Molecular Simulations of Complex Lipid Bilayers. *PLoS Comput. Biol.* **10**, e1003911, (2014).
- 44 Periole, X., Cavalli, M., Marrink, S. J. & Ceruso, M. A. Combining an Elastic Network With a Coarse-Grained Molecular Force Field: Structure, Dynamics, and Intermolecular Recognition. *J. Chem. Theory. Comput.* **5**, 2531-2543, (2009).
- 45 Berendsen, H. J. C., Postma, J. P. M., van Gunsteren, W. F., DiNola, A. & Haak, J. R. Molecular dynamics with coupling to an external bath. *J. Chem. Phys.* **81**, 3684-3690, (1984).
- 46 Tironi, I. G., Sperb, R., Smith, P. E. & van Gunsteren, W. F. A generalized reaction field method for molecular dynamics simulations. *J. Chem. Phys.* **102**, 5451-5459, (1995).
- 47 Hess, B., Bekker, H., Berendsen, H. J. C. & Fraaije, J. G. E. M. LINCS: A linear constraint

- 48 solver for molecular simulations. *J. Comput. Chem.* **18**, 1463-1472, (1997).
- 49 Humphrey, W., Dalke, A. & Schulten, K. VMD: visual molecular dynamics. *J. Mol. Graph.*  
50 **14**, 33-38, 27-38 (1996).
- 51 Hedger, G., Sansom, M. S. P. & Koldsø, H. The juxtamembrane regions of human receptor  
52 tyrosine kinases exhibit conserved interaction sites with anionic lipids. *Sci. Rep.* **5**, 9198,  
53 (2015).
- Hedger, G., Shorthouse, D., Koldso, H. & Sansom, M. S. Free Energy Landscape of Lipid  
Interactions with Regulatory Binding Sites on the Transmembrane Domain of the EGF  
Receptor. *J. Phys. Chem. B* **120**, 8154-8163, (2016).
- 51 Hub, J. S., de Groot, B. L. & van der Spoel, D. g\_wham—A Free Weighted Histogram  
Analysis Implementation Including Robust Error and Autocorrelation Estimates. *J. Chem.*  
*Theory Comput.* **6**, 3713-3720, (2010).
- 52 Notredame, C., Higgins, D. G. & Heringa, J. T-coffee: a novel method for fast and accurate  
multiple sequence alignment1 Edited by J. Thornton. *J. Mol. Biol.* 302, 205-217, (2000).
- 53 Bond, C. S. & Schuttelkopf, A. W. ALINE: a WYSIWYG protein-sequence alignment editor  
for publication-quality alignments. *Acta Crystallographica Section D* 65, 510-512, (2009).

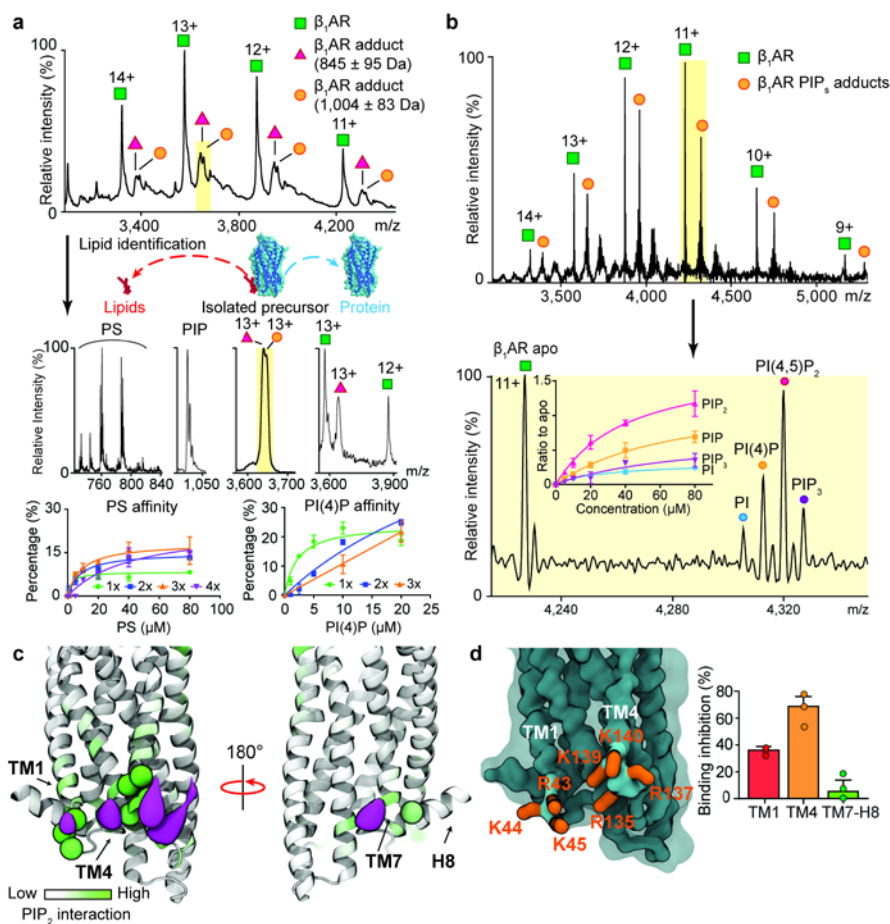


**Figure 1. Identification of endogenous lipids, preferential binding of PI(4,5)P<sub>2</sub>, MD simulation and site-directed mutagenesis define intracellular PIP<sub>2</sub> binding hotspots.** **a**, Charge states of  $\beta_1AR$  (agonist free, 11+ to 14+ green) and adducts are observed bound to the receptor (red, orange). Peaks (highlighted yellow) are selected in the quadrupole and subjected to tandem MS. Phosphatidylserine (PS) and PI(4)P (PIP) were identified in the resulting mass spectra. Binding curves plotted against lipid concentration confirm the preferential binding of PI(4)P over PS. Error bars represent standard deviation of the mean from three independent replicates. **b**, Mass spectra of  $\beta_1AR$  following incubation with an equimolar solution containing PI, PI(4)P, PI(4,5)P<sub>2</sub>, and PI(3,4,5)P<sub>3</sub>. Binding curves confirm favorable binding of PI(4,5)P<sub>2</sub>. Error bars represent standard deviation of the mean from three independent replicates. **c**, CGMD simulation for NTSR1 TM86V- $\Delta$ IC3B embedded in the lipid bilayer containing mixed PC and PIP<sub>2</sub>. Basic residues forming high interaction levels (green spheres) and PIP<sub>2</sub> particle densities (purple surface) representing the most occupied regions (0.6 nm distance cutoff based on the radial distribution of CG particles). **d**, Mutation of residues in NTSR1 (TM86V- $\Delta$ IC3B) highlighted are: TM1 (R43G, K44G and K45G; red), TM4 (R135I, R137T, K139L and K140L; orange) and TM7-H8 (R311N; green). Inhibition of PIP<sub>2</sub> binding is plotted from three independent experiments with standard deviation of the mean. Results indicate that mutations on the TM4 interface have a greater effect than the TM1 and TM7-H8 interfaces.

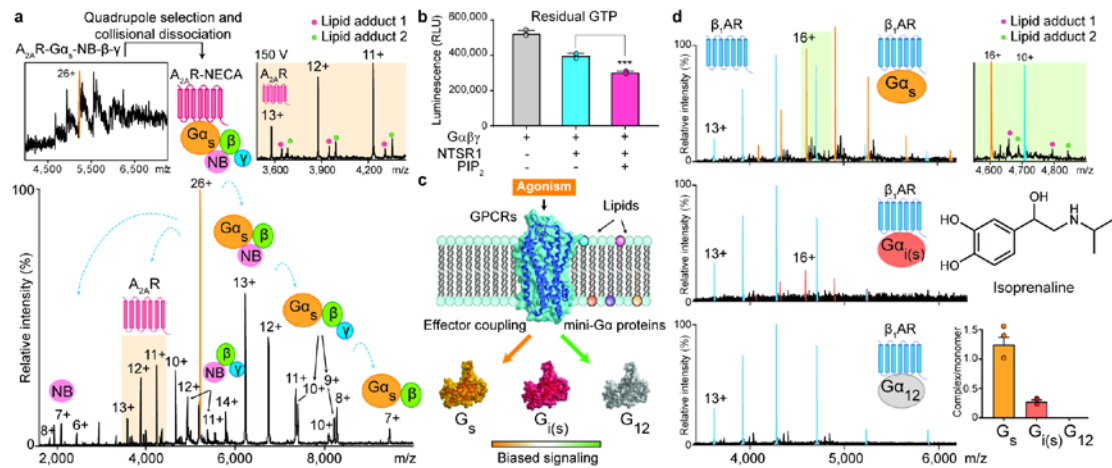


**Figure 2 The selectivity of G-protein coupling and the presence of endogenous lipids on coupled receptors.** **a**, A representative mass spectrum of  $A_{2A}R$  receptor coupled to a trimeric G-protein complex stabilised by a nanobody (Inset top left) from three independent experiments. Isolating and subjecting charge state 26+ (orange main figure) to collision-induced dissociation gives rise to subcomplexes and the liberated receptor with lipid adducts (highlighted orange). **b**, GTPase assays indicate an increase of GTP hydrolysis by active NTSR1 coupled to trimeric  $G\alpha_i\beta\gamma$  in the presence of  $PIP_2$  (\*\*\*) denotes a statistically significant difference ( $p(0.0006) < 0.001$ ) calculated with a t-test to compare the effect of  $PIP_2$  (one variable) on receptor-induced GTPase activation. Data points were overlaid and error bars represent standard deviations of the mean from three independent replicates. **c**, Schematic representation of the influence of lipids and agonists on the binding of mini-G proteins. **d**, Mass spectra of isoprenaline bound  $\beta_1AR$  with three different mini-G subunits (mini- $G_s, i(s), 12$ ). Enhanced coupling and lipid adducts are observed in the presence of  $G_s$  (highlighted green top right). Error bars denote standard deviations of the mean from three independent replicates and each data point was overlaid.

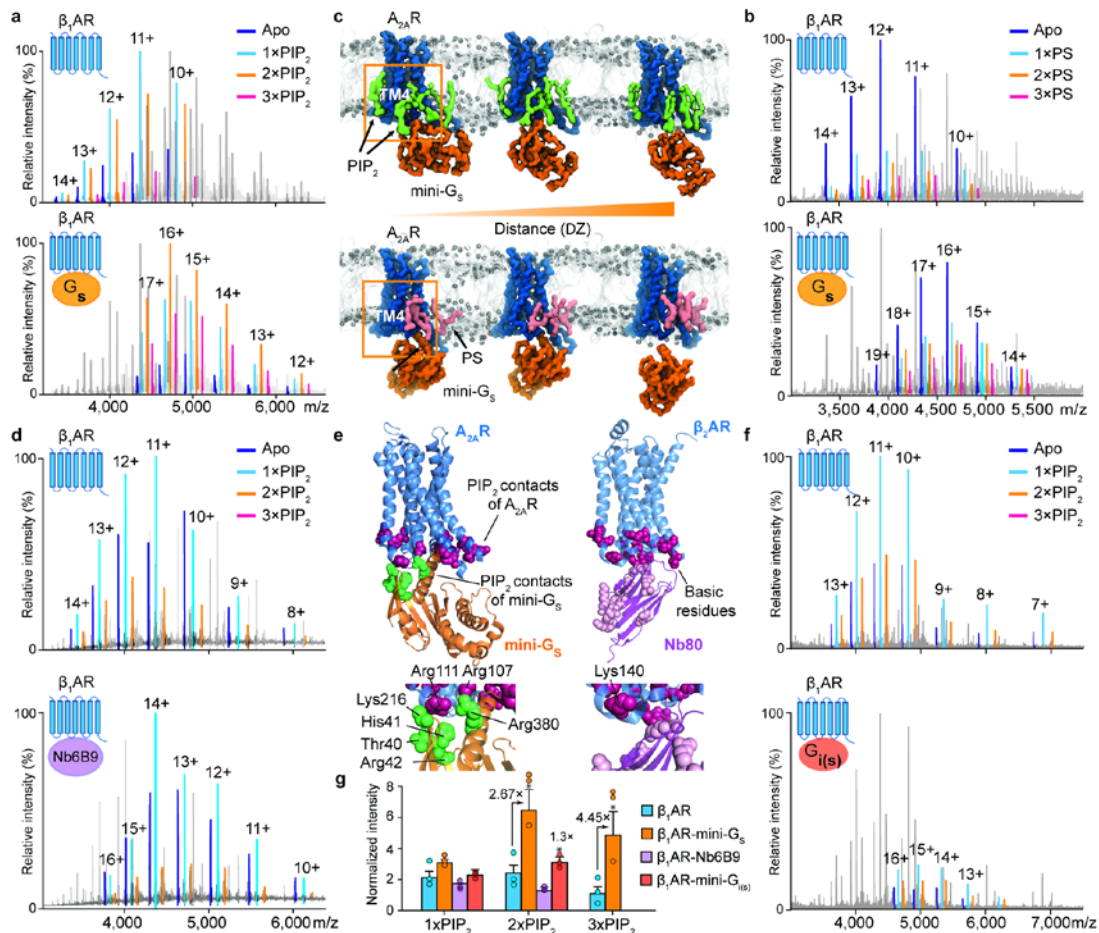


**Figure 3** The effect of PIP<sub>2</sub> on coupling to mini-G<sub>s</sub>, and comparison with PS, a nanobody and mini-G<sub>i</sub>. **a**, A representative mass spectrum of the  $\beta_1$ AR:mini-G<sub>s</sub> complex (n=3) in the presence of PIP<sub>2</sub> and the agonist isoprenaline with uncoupled  $\beta_1$ AR lipid bound states highlighted according to the colour coding (upper) and  $\beta_1$ AR:mini-G<sub>s</sub> lipid bound states highlighted in the same spectrum (lower). **b**, A representative mass spectrum of the  $\beta_1$ AR:mini-G<sub>s</sub> complex (n=3) in the presence of PS and the agonist isoprenaline. No appreciable difference can be attributed to PS binding between  $\beta_1$ AR and  $\beta_1$ AR:mini-G<sub>s</sub>. **c**, Snapshots of steered MD simulations to pull mini-G<sub>s</sub> away from A<sub>2A</sub>R in the presence of PIP<sub>2</sub> (green) and PS (pink). Results reveal different binding modes of PIP<sub>2</sub> and PS to the receptor (outlined orange boxes). The interaction of mini-G<sub>s</sub> with A<sub>2A</sub>R is stabilised in the presence of PIP<sub>2</sub> by ~50 kJ/mol relative to PS (Extended Data Fig. 6b). **d**, A representative mass spectrum recorded following incubation of  $\beta_1$ AR with PIP<sub>2</sub>, isoprenaline and a nanobody (Nb6B9) (0.3 molar ratio to receptor, n=3). **e**, PIP<sub>2</sub> contacts of A<sub>2A</sub>R-miniG<sub>s</sub> complex are shown on the receptor (purple) and miniG<sub>s</sub> (Thr40, His41, Arg42, Lys216, Arg380; green), and juxtaposed to basic residues on  $\beta_2$ AR-Nb80 complex (purple). **f**, A representative mass spectrum of PIP<sub>2</sub> binding to mini-G<sub>i(s)</sub> (n=3). No difference is detected +/- PIP<sub>2</sub>. **g**, The intensity ratios of different lipid bound states to the apo state of receptor in the uncoupled/coupled state are plotted. The asterisk denotes a statistically significant difference (p < 0.05) calculated as one-way ANOVA with Dunnett's multiple comparison test. Error bars represent standard deviations of the mean from three independent replicates.

**Extended Data Figure 1. Identification of lipids bound to NTSR1 HTGH4- $\Delta$ IC3B.** a, Endogenous lipid bounds to NTSR1 HTGH4- $\Delta$ IC3B, isolated from *E. coli*, are identified as PA following m/z selection in the MS quadrupole of the NTSR1:lipid 11+ charge state (highlighted yellow) and collisional activation to dissociate PA and its homologues (m/z 700–760 Da). b, Lipidomics analysis of purified NTSR1 with three technical replicates reveals peaks at low m/z. MS/MS spectra of the precursor ion [M-H-1] at m/z 699.32 highlighted yellow, leads to definitive fragment ions at m/z 281 and 417 consistent with the structure of PA (36:2). c, Analogous lipidomics analysis of purified  $\beta_1$ AR from insect cells with three technical replicates. MS/MS spectra of the two [M-H-1] precursor ions (m/z 758.50 and 786.53) identified the lipids as PS (34:2) and PS (36:2) respectively with diagnostic fragments indicated.

**Extended Data Figure 2. Lipid binding preference of NTSR1 and  $\beta_1$ AR.** The binding of NTSR1 HTGH4- $\Delta$ IC3B, measured by mass spectrometry (n=3), to the phospholipids PA (a), PS (b), PI (c), PC (d) and DAG (e). The measurements were performed at different lipid concentration (0 to 160  $\mu$ M) and the percentages of individual lipid-binding peaks (sum of apo protein and all lipid adducts obtained in the region of the mass spectrum under study) were plotted against lipid concentrations in solution. The lipid-binding curves were deduced from fitting to one-site total binding (GraphPad Prism software). Standard deviations of the mean were calculated from three independent replicate experiments at each concentration. The results show that NTSR1 interacts preferentially with anionic phospholipids (PA and PS) as no binding was observed for neutral (DAG) and zwitterionic (PC) lipids. Exogenous POPS (f) and PI(4)P (g) were added to  $\beta_1$ AR at different final concentrations (10  $\mu$ M shown here). Spectra were recorded for a range of lipid concentrations from 0 – 80  $\mu$ M for PS and 0 – 20  $\mu$ M for PI(4)P. Peak intensities of the individual PI(4)P-bound species were measured and plotted against lipid concentration to yield a relative affinity for one PI(4)P binding (1x), two PI(4)P molecules binding (2x) or three PI(4)P molecules binding (3x); only the first PI(4)P molecule binds with high affinity (see Fig. 1a). Error bars represent the standard deviation of the mean between three independent experiments.

**Extended Data Figure 3. Investigation of the phospholipid preferences of  $A_2A$ R and NTSR1.** a, A representative mass spectrum of purified  $A_2A$ R from three independent experiments revealed truncations of the N-terminal sequence (MPIM). The arrow between each species refers to the mass differences corresponding to truncated amino acids (M, PI and M). b, A competitive binding assay (n=3) in which  $A_2A$ R was incubated with a mixture of lipids (PI, PI(4)P, PI(4,5)P<sub>2</sub>, and PI(3,4,5)P<sub>3</sub>) prior to MS, indicated that PIP<sub>2</sub> binds with a higher affinity than other phospholipids to  $A_2A$ R. c, The analogous competitive binding assay in which NTSR1 was incubated with a mixture of lipids (PI, PI(4)P, PI(4,5)P<sub>2</sub>, and PI(3,4,5)P<sub>3</sub>) prior to MS. Ratio to apo is plotted as a function of concentration and defined as the intensity ratio of individual PIP adducts to the receptor in the apo state. The same data analysis methods are used for Fig. 1b. Results indicate that PIP<sub>2</sub> binds with a higher affinity than other phospholipids to  $A_2A$ R. Error bars represent standard deviation of the mean from three independent replicates. d, A representative mass spectrum of  $A_2A$ R (n=3) used for preparation of the G protein complex reveals lower abundance of PS and PI adducts prior coupling to G proteins.

**Extended Data Figure 4. NTSR1- and  $\beta_1$ AR-PIP<sub>2</sub> interactions within CGMD simulations and comparison of PIP<sub>2</sub> contacts over different GPCRs. a,**

Volumetric density surfaces showing the average spatial occupancy of PIP<sub>2</sub> lipids around a crystal structure of NTSR1 TM86V- $\Delta$ IC3B (PDB: 4BUO), which shares a greater sequence identity to the wild-type receptor (91%) than NTSR1 HTGH4- $\Delta$ IC3B (86%), contoured to show the major PIP<sub>2</sub> interaction sites. Density surfaces were calculated over 5- $\mu$ s of CGMD (blue surface, n=10 independent experiments), and 100- $\mu$ s of CGMD (magenta, n=1 independent experiment). The cytoplasmic side of NTSR1 structure is colored from white (low PIP<sub>2</sub> interaction) to red (high PIP<sub>2</sub> interaction). Extending a simulation to 100  $\mu$ s revealed no overall change in the patterns of PIP<sub>2</sub> interaction. Less specific, and hence more dynamic, interaction was seen for the acyl chain moieties of PIP<sub>2</sub>, which yielded more diffuse probability densities. **b,**  $\beta_1$ AR-PIP<sub>2</sub> interactions within CGMD simulations. Contact patterns are shown for simulations containing 5% PIP<sub>2</sub> in the lipid bilayer and thermostable  $\beta_1$ AR (PDB: 2Y03, upper panel), 10% PIP<sub>2</sub> and thermostable  $\beta_1$ AR (middle panel), and 10% PIP<sub>2</sub> and S68R  $\beta_1$ AR construct (bottom panel). In each case PIP<sub>2</sub> contacts were calculated over 5- $\mu$ s of CGMD (n=10 independent experiments), with each repeat simulation initiated from different random system configurations. The std of the mean of lipid contact number is denoted by black error bars. **c,** PS and PIP<sub>2</sub> contacts with NTSR1 as a function of residue position, for PC:PS membranes (top left), PC:PS:PIP<sub>2</sub> membranes (top right), PC:PIP<sub>2</sub> membrane (bottom left) and PC:PS:PIP<sub>2</sub> (bottom right). The position of helices is denoted by horizontal grey bars. Lipid contact is calculated as the mean number of contacts between each residue and a given lipid species per frame, using a 6 Å distance cut-off. Error bars (black) denote the standard deviation of the mean between simulation repeats (n=3). **d,** PIP<sub>2</sub> contacts seen in CG MD simulations for nine Class A GPCRs (3RZE = histamine H1 receptor; 2VT4 =  $\beta_1$  adrenergic receptor; 2RH1 =  $\beta_2$  adrenergic receptor; 5TGZ = CB1 cannabinoid receptor; 5DSG = M4 muscarinic acetylcholine receptor; 3EML = adenosine A<sub>2A</sub> receptor; 3PBL = dopamine D3 receptor; 3V2W = sphingosine 1-phosphate receptor; 1F88 = rhodopsin). The sequences of the GPCRs are shown, with the TM helices, intracellular loops (ICL) and H8 helices indicated by horizontal bars, and with amino acids coloured by their mean number of contacts per simulation frame with the PIP<sub>2</sub> molecules. The three green boxes correspond to the high frequency of PIP<sub>2</sub> interactions discussed in the main text for the NTSR1, for the TM1, TM4, and TM7/H8 motifs. Contacts were computed over 1  $\mu$ s CG-MD simulations (n=3 independent experiments) for each GPCR, using a 6 Å cut-off. Sequences were aligned using T-Coffee<sup>52</sup> and mapping of protein-lipid contact data onto the sequence alignment used ALINE<sup>53</sup>.

**Extended Data Figure 5. Site-directed mutagenesis attenuates PIP<sub>2</sub> binding to NSTR1. a,**

Schematic representation of the experimental protocol designed to combine MS with mutagenesis to produce mutants of lower molecular mass than wild type which when incubated with PIP<sub>2</sub> yield a direct readout of the effect of mutations in specific regions. **b,** PIP<sub>2</sub>-binding of NTSR1 mutants on residues that exhibit the highest frequency of PIP<sub>2</sub> interaction in MD simulation. Mutation of NTSR1 HTGH4- $\Delta$ IC3B residues on TM1 (R46G, K47G and K48G (R43G, K44G and K45G in NTSR1 TM86- $\Delta$ IC3B; R91G, K92G, K93G in wild-type); red bar), TM4 (R138I, R140T, K142L and K143L (R135I, R137T, K139L and K140L in NTSR1 TM86- $\Delta$ IC3B; R183I, R185T, K187L and K188L in wild-type); orange bar) and TM7-H8

(R316N (R311N in NTSR1 TM86- $\Delta$ IC3B; R377N in wild-type); green bar) attenuate PIP<sub>2</sub> binding, and indicates that the TM4 interface is a preferential binding site over TM1 and TM7-H8 interfaces. The selection of residues for mutations was guided by MD (Extended Data Figure 4) and previous studies wherein binding of a fluorescence-labeled agonist, BODIPY neurotensin, to NTSR1, was screened and used to monitor efficient production, insertion, and folding<sup>10</sup>.

**Extended Data Figure 6. PIP<sub>2</sub> binds preferentially to  $\beta_1$ AR in an active state and stabilises  $\beta_1$ AR coupled to mini-G<sub>s</sub> and A<sub>2A</sub>AR-mini-G<sub>s</sub> complex.**

**a**, A time course experiment was performed to capture the complex formation of mini-G<sub>s</sub> and active  $\beta_1$ AR as a function of time. The coupling efficiency (percentage) was calculated from the relative intensity of peaks assigned to the  $\beta_1$ AR coupling to mini-G<sub>s</sub> at the appropriate lipid-bound state. The plot indicates that mini-G<sub>s</sub> coupling is enhanced by PIP<sub>2</sub> when more than two lipids are bound to the receptor. Error bars represent standard deviations of the mean from at least three independent experiments. **b**, Plot of potential of mean force (PMF) for the interaction of mini-G<sub>s</sub> with A<sub>2A</sub>AR in the presence of PIP<sub>2</sub> (green curve) and PS (grey). The PMF is calculated along a reaction coordinate ( $\Delta z$ ) corresponding to the centre-centre separation of the mini-G<sub>s</sub> and receptor proteins along the z-axis (normal to the bilayer plane). The interaction of mini-G<sub>s</sub> with the A<sub>2A</sub>AR is stabilised in the presence of PIP<sub>2</sub> by  $\sim 50 \pm 10$  kJ/mol relative to PS. The error bars on the figure (which are less than 10 kJ/mol) are from bootstrap sampling of the PMFs and thus are the ‘statistical’ errors in estimating the well depth from a given set of simulations/PMF calculation (n=3 independent experiments). A minimum error of  $\leq \sim 10$  kJ/mol is therefore estimated. **c**, Mass spectra were recorded for a 1:1 equimolar mix of an inactive unliganded  $\beta_1$ AR variant E130W and its unmodified active counterpart (co-purified with the agonist isoprenaline) in the presence of PI(4,5)P<sub>2</sub>. Lipid binding occurred on both receptors but following normalization to account for differences in ionization efficiency a clear preference for PIP<sub>2</sub> binding to the active receptor was observed. (Error bars denote standard deviation of the mean between three independent experiments).

**Extended Data Figure 7. Detection of nanobody coupling to  $\beta_1$ AR.** Mass spectral peaks assigned to the nanobody (Nb6B9) binding to  $\beta_1$ AR to form a  $\beta_1$ AR·Nb6B9 complex at an equimolar ratio are highlighted (orange) and demonstrate complete complex formation implying a higher affinity of the nanobody than mini-G<sub>s</sub> for  $\beta_1$ AR (N=3 independent experiments).

**Extended Data Figure 8. Structural comparison of class A and class B GPCRs in complex with trimeric G $\alpha\beta\gamma$  complexes.** The PIP<sub>2</sub> contacts of the G $\alpha_s$  subunit observed in MD simulation (green spheres) were highlighted on the structures of trimeric G interactions with  $\beta_2$ -adrenergic receptor ( $\beta_2$ AR) (PDB: 3SN6), the glucagon-like peptide-1 receptor (GLP-1) (PDB: 5VAI), and the calcitonin receptor (CTR) (PDB: 5UZ7). The basic residues on the interface adjacent to the cytoplasmic end of TM4 are also highlighted (purple spheres). Expansion indicates the conserved pattern of PIP<sub>2</sub> bridging in class A GPCRs ( $\beta_2$ AR and A<sub>2A</sub>AR (Fig. 3e)) both of which have basic residues on TM4 (Lys140 and Arg107/111) which are not observed in class B GPCRs GLP-1R and CTR.

**Table 1. Lipidomics analysis of purified  $\beta_1$ AR**

**Table 2. Simulations run. Lipids were symmetrically distributed between leaflets.**